Hexagonal Boron Nitride Vacancies as an Enhanced Single Photon Source

Guy Leckenby

Supervisor: Marcus Doherty

PhB Advanced Studies Extension, Research School of Physics & Engineering
The Australian National University, Canberra, ACT 2611, Australia

April 10, 2017

Abstract

Single photon sources are highly sought after as the first building blocks in a wide variety of quantum technologies. We present hexagonal boron nitride (hBN) defects as a potential single photon source for use in such applications. hBN is a promising single photon source due to its 2-dimensional resilient structure, narrow zero phonon line, and ultrabright count rate of 4.2×10^6 counts s^{-1}. Furthermore, we demonstrate the design of a high finesse fibre microcavity which can be coupled to hBN to enhance the spontaneous emission rate via the Purcell effect. By analysing this coupling, we deduce that a maximum Purcell factor of 14.41 is attainable at a cavity length of 0.3115 μm. Thus we conclude that cavity enhancement of single photon sources has the potential for order of magnitude increase in count rate.

I. Introduction

Quantum technologies have gathered extensive interest over the past few decades for the ability to revolutionise cryptography, computation speed and information transfer. However the large majority of these applications inherently require a stable single photon source (SPS) that can be triggered on demand. These purely quantum properties are difficult to access and have only recently even been observed with the first observations of photon counting statistics occurring just 40 years ago (Kimble et. al., 1977). Today there are numerous processes available including diamond vacancy centres, quantum dots, carbon nanotubes, and florescence of a wide range of other quantum systems (Aharonovich et. al., 2011).

Single photons are used broadly in quantum applications because their quantum states are easily manipulable (e.g. polarisation), they are weakly interacting thus preserving quantum states over long distances, and are energy efficient in production (although some SPSs require significant energy input). In particular polarisation states are easy to manipulate and are thus used widely in simple implementations of quantum technologies. In quantum cryptography, quantum key distribution uses polarization of single photons as the transmission mechanism for both BB84 or B92 encryption protocols and entangled state cryptography (Naik et. al., 2000). Most of the basic implementations of qubits for quantum computing require single photon sources which are manipulated by linear optical components. More advanced methods like NMR systems, ion traps, quantum dots and superconducting systems use trapped photons rather than SPSs (Fox, 2006). SPSs can also be used to test Bell's inequality and investigate quantum teleportation through the Hong-Ou-Mandel interferometer (Fox, 2006).

An ideal single photon source emits one photon on demand. In quantum cryptography, any deviation from a single photon generates error and potential for successful eavesdropping (Fox, 2006). In quantum computing, multiple photons introduce extra states which alters the effects of quantum gates on qubits. However there are several other metrics that constitute the suitability of an ideal SPS. Aharonovich et. al. (2011) focus on six important factors:

1) Stable emission, that is free from blinking (varying intensity) or bleaching (reduction of luminescence due to other reactions).
2) A narrow phonon linewidth with the majority of luminescence in the zero phonon line providing indistinguishable photons
3) A short excited state lifetime ($ps < \tau < ns$) for better antibunching rates.
4) Fully polarised in absorption and emission channels which is required for practical quantum cryptography.
5) Two level system with non shelving or metastable state generating reliable radiative emission.
6) Negligible dephasing and spectral diffusion to produce enduring identical photons.

Whilst there is no perfect SPS, there are many systems which make good approximations. Each has their own advantages and disadvantages, however one system type that is attracting extensive research currently are vacancy centres because of their photostable emission, room temperature operation and long coherence times (Aharonovich et. al., 2011).

II. hBN as a Single Photon Source

This report will focus on nitrogen vacancies in hexagonal boron nitride (hBN). hBN is of particular interest as it was the first two-dimensional material to demonstrate room temperature single photons and generates both polarised and ultra bright emission (Tran et. al., 2015). This 2 dimensionality is important for compact applications such a photonic circuits on single chips. The large bandgap of hBN allows for defects with relatively narrow zero phonon linewidths of about $10\,nm$ at room temperature (Tran et. al., 2015). Furthermore the defects are localised for precise applications and are highly robust, being able to withstand aggressive annealing in both oxidising and reducing environments (Tran et. al., 2016). This
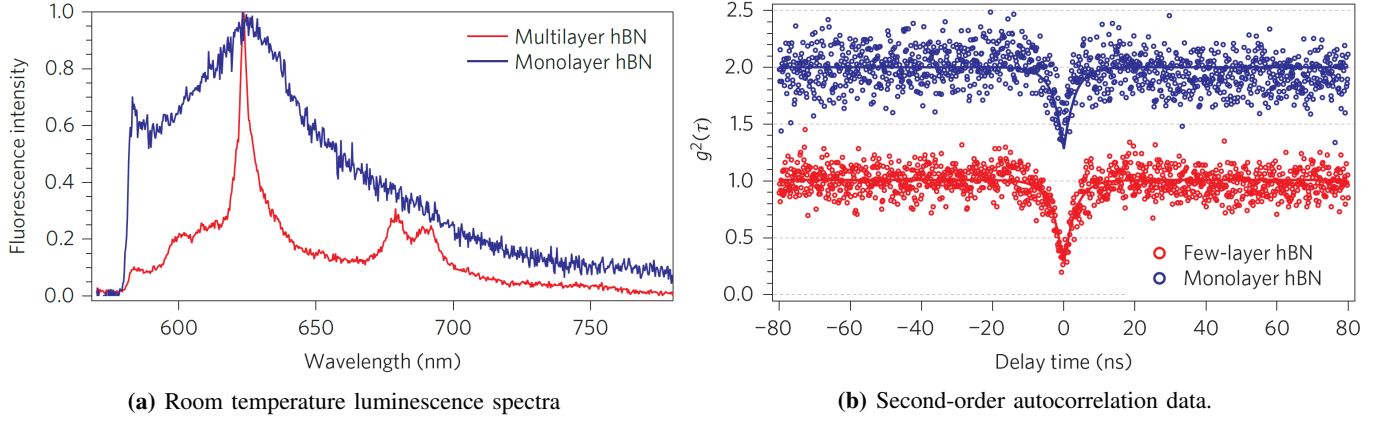
(a) Room temperature luminescence spectra

(b) Second-order autocorrelation data.

Figure 1: Spectroscopic data of a localised defect for mono- and multilayer hBN (Tran et. al., 2015).

sets hBN up as an important SPS for quantum information and nanophotonic applications.

hBN has a wide bandgap of $6\,eV$ which houses several defects. Tran et. al. (2015) identified three candidates for the observed optical defects; a nitrogen vacancy (V_N), a boron vacancy (V_B), or an anti-site complex where a nitrogen occupies a boron site and the nitrogen site is left vacant ($N_B V_N$). By modelling band gap transitions, Tran et. al. (2015) concluded that the $N_B V_N$ defect is the most probable candidate for the observed optical emission and that the other vacancies will emit at non-optical wavelengths. The structure of the $N_B V_N$ defect in the 2D hBN lattice is seen in Figure 2.
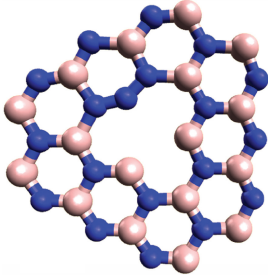
Figure 2: Molecular structure of the $N_B V_N$ defect within the hBN lattice (Tran. et. al., 2015).

The observed spectrum (Tran et. al., 2015) of the $N_B V_N$ defect in hBN (hereby we shall refer to $N_B V_N$ as simply the defect) is shown in Figure 1a. In both the mono- and multilayer cases, a bright peak is observed at $\sim 623\,nm$. In the monolayer case, it is significantly broadened and asymmetric which is not ideal for SPS applications. However the dominant excitation peak narrows significantly in the multilayer case where the zero phonon line (ZPL) has a FWHM of $\lesssim 10\,nm$. The multilayer defect also exhibits a phonon side band (PSB) doublet at $680\,nm$ and $693\,nm$ which yields a Debye-Waller (DW) factor of ~ 0.82 which is among the highest for vacancy centres. Simple NV centres in diamond have DW factors of 0.04 however SiV and CrV can demonstrate DW factors as high as 0.8 (Aharonovich. et. al., 2011).

SPSs are traditionally tested using Hanbury, Brown, & Twiss (HBT) interferometry to measure the second-order autocorrela-

tion function $g^{(2)}(\tau)$. Fitting Eqn (1) to the data from Figure 1b, Tran et. al. (2015) found lifetimes of $\tau_1 \simeq 2.5\,ns$ and $\tau_2 \simeq 22.2\,ns$. τ_1 is the lifetime of the emitting state, which is of primary interest to determine the emission rate of the SPS, whilst τ_2 is the lifetime of the metastable state. Tran et. al. (2015) used an extended three level model, pictured in Figure 3, which produces an autocorrelation function of the form

$$g^{(2)}(\tau) = 1 - (1+A)\exp\left(-\frac{|\tau|}{\tau_1}\right) + A\exp\left(-\frac{|\tau|}{\tau_2}\right) \quad (1)$$

where τ_1 and τ_2 are the lifetimes of the excited and shelving states respectively. A true SPS exhibits a value of $g^{(2)}(0) < 0.5$ and we see that for both the mono- and multilayer case, the defect satisfies this.

Tran et. al. (2015) also fitted the emission intensity as a function of excitation power using a relationship given by

$$I = I_\infty \frac{P}{P + P_{\text{sat}}} \quad (2)$$

where I_∞ and P_{sat} are the emission rate and excitation power at saturation respectively. They got results of $I_\infty = 4.2 \times 10^6$ counts s^{-1} and $P_{\text{sat}} = 611\,\mu W$ which are the brightest for any vacancy centre in the visible spectrum and are comparable with the brightest quantum emitters in general. However as hBN outperforms these other vacancy centres in robustness, availability and purity, we expect hBN to receive extensive characterisation and implementation in the future.
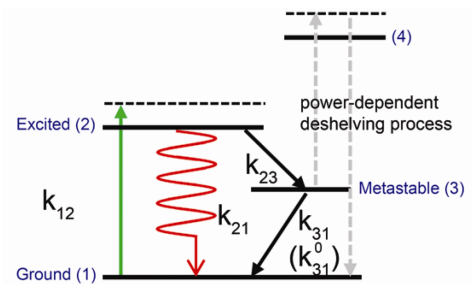
Figure 3: The extended three level model for the hBN defect used by Tran et. al. (2015).

III. CAVITY ENHANCEMENT

Alongside the single photon sources themselves, microcavities are attracting attention due to their ability to enhance the desirable properties of the SPSs. In particular, the Purcell effect can be used to enhance the spontaneous emission rate of the SPS. This reduces the relaxation time after excitation which in turn produces a more controlled and regular emission of photons.

Depending on the parameters of the cavity, the cavity modes will either be close to or far from resonance for the considered transition. In particular, the photon density of states will be higher near cavity modes and thus the probability of spontaneous emission will be higher near cavity modes. This serves to either suppress or enhance the spontaneous emission of system (Fox, 2006). This effect, known in the weak coupling regime as the Purcell effect, can be succinctly expressed in the Purcell Factor which is a comparison of the spontaneous emission rate for the cavity with free space:

$$F_P \equiv \frac{\tau_R^{\text{free}}}{\tau_R^{\text{cav}}} = \frac{3Q(\lambda/n)^3}{4\pi^2 V_0} \int \frac{\xi^2 \Delta\omega_c^2 \mathcal{L}(\omega_0)}{4(\omega_0 - \omega_c)^2 + \Delta\omega_c^2} \mathrm{d}\omega_0 \quad (3)$$

where $\mathcal{L}(\omega_0)$ is the transition lineshape, ω_0 the transition frequency and ω_c the cavity mode frequency, Q the quality factor, V_0 the cavity volume, λ the free-space wavelength of the transition, n the refractive index of the cavity, and ξ is the is the normalised dipole orientation factor. Values of $F_P > 1$ imply enhanced spontaneous emission whilst $F_P < 1$ implies suppressed emission.

IV. FIBRE MICROCAVITIES

Albrecht et. al. (2013) have demonstrated an enhancement of a NV centre with a fibre-based microcavity, depicted in Figure 4. The cavity consists of a floating plane mirror which has been coated to yield a very high reflectivity ($R_{1,ZPL} = 0.99995$) at the ZPL of the defect but less than 5% at $532\,nm$. The second mirror is a concave shape coated such that $R_{2,ZPL} = 0.999$ and $R_{2,532} = 0.9999$. This allows the excitation laser to enter the cavity but ensures the dominant output channel is from the ZPL. At these high reflectivities, the theoretically calculated finesse is as high as $\mathcal{F}_{\text{theo}} \simeq 6000$ however when the losses of the system are taken into account, this number drops to $\mathcal{F}_{\text{obs}} = 3600 \pm 600$.

To provide the nitrogen vacancy centres required to produce a SPS, Albrecht et. al (2013) applied a solution of diamond nanocrystals to the surface of the plane mirror by spin coating. The fact that the floating mirror is controlled by piezo-stepper motors then allowed them to align the nanodiamonds with the excitation laser such that the the focus point of the hemispherical mirror aligned with the nanodiamond generating the required cavity coupling. The fibre containing the hemispherical mirror was mounted on a purpose built piezo-driven flexure device that can control the cavity. As we will discover, this is crucial to optimising the Purcell Factor.

Due to the presence of the concave mirror, the microcavity presented by Albrecht et. al. (2013) slightly differs from a traditional Fabry-Pérot cavity. However Fabry-Pérot cavities are the simplest to analyse as they are plane parallel mirrors
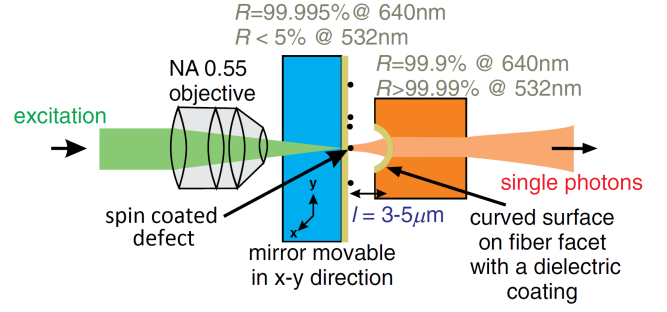

Figure 4: A fibre microcavity consisting of a concave mirror imprinted in a fibre facet and a plane mirror with defects attached.

in opposition. As the concave mirror will only increase the photon density of states (and thus enhance the Purcell effect), we will analyse this microcavity as a Fabry-Pérot cavity. The cavity modes of a Fabry-Pérot cavity are those that generate standing waves for the light inside the cavity. In particular, the angular frequencies of the resonant modes are given by $\omega_m = m\pi c/n L_{\text{cav}}$ (where m is an integer) with the spectral width given by $\Delta\omega = \pi c/n\mathcal{F}L_{\text{cav}}$ where $\mathcal{F}$ is the finesse of the cavity given by $\mathcal{F} = \pi(R_1 R_2)^{\frac{1}{4}}/(1 - \sqrt{R_1 R_2})$. As the input beam is Gaussian, we will assume that transverse modes inside the cavity will be dominated by the fundamental TEM_{00} mode which is centred on the defect. Because we will consider the mode to have a diffraction limited waist, the modal volume associated will be $V_0 = A_0 L_{\text{cav}}$ where $A_0 = \pi\lambda^2/4$.

Implementing the values provided by Albrecht et. al. (2013) as a prototype microcavity, we notice that the linewidth of the cavity, for an approximate cavity length of $L_{\text{cav}} = 3\,\mu m$, is $\Delta\omega_c = 8.72 \times 10^{10}$. This is significantly smaller than the linewidth of the ZPL $\Delta\omega_0 \approx 5 \times 10^{13}$ and thus we can approximate the Lorentzian cavity modes as a delta function;

$$\frac{\Delta\omega_c}{4(\omega_0 - \omega_c)^2 + \Delta\omega_c^2} = 2\pi\delta(\omega_0 - \omega_c).$$

By definition, $Q = \omega_c/\Delta\omega_c$ and $V_0 = A_0 L_{\text{cav}}$ where A_0 is the modal area associated with the cavity defined above. For optimum enhancement, the cavity mode is aligned with the transition dipole moment of the defect such that $\xi = 1$. The microcavities are also filled with air so we take $n = 1$. Using the above definitions, the expression for the Purcell factor can be simplified to

$$F_P = \frac{3\,c\,\lambda^3}{2A_0} \sum_m \frac{m}{L_{\text{cav}}^2} \mathcal{L}(\omega_c) \quad (4)$$

which is a function of cavity length. This analysis can now be applied to the hBN system.

V. CAVITY ENHANCEMENT OF hBN

From Figure 1a, it is clear that the ZPL is a Lorentzian lineshape which dominates the multilayer spectrum. Hence to determine the Purcell effect on hBN, we shall approximate $\mathcal{L}(\omega)$ as just the ZPL giving

$$\mathcal{L}(\omega) = \frac{\Gamma/2}{(\omega - \omega_0)^2 + (\Gamma/2)^2}.$$
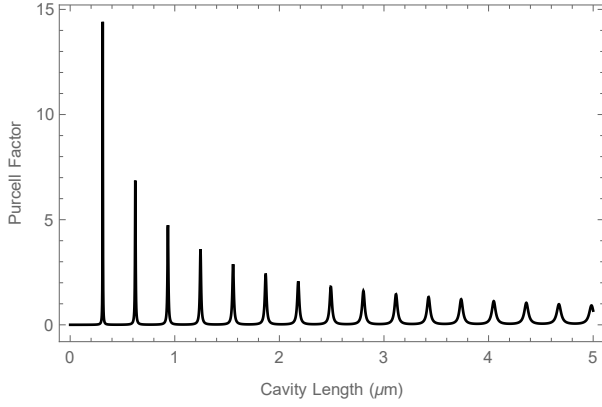
Figure 5: The Purcell factor as a function of the cavity length for hBN.

where we have $\Gamma = 31.90\,THz$ and $\omega_0 = 3024\,THz$ as measured from Figure 1a. Given that $A_0 = \pi\lambda^2/4$, this produces a Purcell Factor of

$$F_P = \frac{3c\lambda}{8\pi}\sum_m \frac{m}{L_{\text{cav}}^2}\frac{\Gamma/2}{(\omega_c - \omega_0)^2 + (\Gamma/2)^2}, \qquad (5)$$

with ω_c and $\Delta\omega_c$ defined above, which is a function of the cavity length. The plot is given in Figure 5 which demonstrates how the Purcell factor peaks at the cavity modes before returning to approximately zero in between. Hence if a cavity is to be introduced, the length needs to be highly accurate otherwise the Purcell effect could generate a suppression of the spontaneous emission rather than an enhancement.

Using this formulation, we conclude that the cavity length which maximises the Purcell effect is $L_{\text{cav}} = 0.3115\,\mu m$ corresponding to a Purcell factor of $F_P = 14.41$. Given that hBN emits single photons at a maximum rate of $4.2 \times 10^6\,\text{counts}\,s^{-1}$, the enhanced emission rate will be $I_{\text{enh}} = F_P\,I_\infty = 6.052 \times 10^7\,\text{counts}\,s^{-1}$. Whilst this is an upper bound on the single photon generation of the hBN-microcavity system, it predicts that we can realistically generate count rates 10 times higher than any naked SPS.

VI. CONCLUSION

In this report, we have established the technological applications for single photon sources and described the properties of an ideal single photon source. Following Tran et. al. (2015), hexagonal boron nitride was introduced as a two dimensional SPS as a result of anti-site complex defects embedded within the bandgap. Whilst mono-layer hBN had a significantly broadened emission spectrum, the multi-layer formulation demonstrated a narrow zero phonon line at $623\,nm$ with a linewidth of approximately $7\,nm$ and relatively minimal phonon side bands. The hBN defect had a Debye-Waller factor of ~ 0.82 which is among the highest available currently for SPSs. The count rate observed was $I_\infty = 4.2 \times 10^6\,\text{counts}\,s^{-1}$ which is again amongst the highest available SPSs. Combined with the fact that hBN is a highly durable and reproducible material, as demonstrated by Tran et. al. (2016), it establishes hBN as an important candidate for economical implementation in quantum technologies.

We also investigated how cavities can be used to enhance the spontaneous emission of SPSs via the Purcell effect. In particular we investigated a fibre microcavity presented by Albrecht et. al. (2013) and analysed how such a Fabry-Pérot cavity could enhance the emission rate of a SPS. We concluded that such a cavity could produce a Purcell factor of up to $F_P = 14.4$ given a very well aligned cavity length of $L_{\text{cav}} = 0.3115\,\mu m$. This would increase the count rate for hBN to $I_{\text{enh}} = 6.05 \times 10^7$. This count rate is 10 times larger than any yet quoted in the literature and could be improved by optimising the cavity parameters. With such highly durable, ultrabright and cost efficient single photon sources becoming available, economical implementations of quantum technologies could become a reality within the next few decades.

REFERENCES

Aharonovich, I., Castelletto, S., Simpson, D.A., Su, C-H., Greentree, A.D., & Prawler, S. 2011. 'Diamond-based single-photon emitters,' *Reports on Progress in Physics,* vol. 74 076501 (28pp).

Albrecht, R., Bommer, A., Deutsch, C., Reichel, J., & Becher, C. 2013. 'Coupling of a Single Nitrogen-Vacancy Centre in Diamond to a Fibre-Based Microcavity,' *Physical Review Letters,* vol. 110, 243602.

Fox, M. 2006. *Quantum Optics: An Introduction*, Oxford University Press, Oxford, NY.

Kimble, H.J., Dagenais, M., & Mandel, L. 1977. 'Photon Antibunching in Resonance Fluorescence,' *Physical Review Letters,* vol. 39, no. 11, pp. 691-5.

Naik, D.S., Peterson, C.G., White, A.G., Berglund, A.J., & Kwiat, P.G. 2000. 'Entangled State Quantum Cryptography: Eavesdropping on the Ekert Protocol,' *Physical Review Letters*, vol. 84, no. 20, 4733-6.

Tran, T.T., Bray, K., Ford, M.J., Toth, M. & Aharonovich, I. 2015. 'Quantum emission from hexagonal boron nitride monolayers,' *Nature: Nanotechnology,* vol. 11, pp. 37-41.

Tran, T.T., Elbadawi, C., Totonjian, D., Lobo, C.J., Grosso, G., Moon, H., Englund, D.R., Ford, M.J., Aharonovich, I., & Toth, M. 2016. 'Robust multicolour single photon emission from point defects in hexagonal boron nitride,' *ACS Nano*, vol. 10, -p. 7331-8.